

Mixed axion-wino dark matter

Kyu Jung Bae^a, Howard Baer^a, Andre Lessa^b and Hasan Serce^a

^a*Dept. of Physics and Astronomy, University of Oklahoma, Norman, OK 73019, USA*

^b*Instituto de Física, Universidade de São Paulo, São Paulo - SP, Brazil*

E-mail: bae@nhn.ou.edu, baer@nhn.ou.edu, lessa@if.usp.br, serce@ou.edu

ABSTRACT: A variety of supersymmetric models give rise to a split mass spectrum characterized by very heavy scalars but sub-TeV gauginos, usually with a wino-like LSP. Such models predict a thermally-produced underabundance of wino-like WIMP dark matter so that non-thermal DM production mechanisms are necessary. We examine the case where theories with a wino-like LSP are augmented by a Peccei-Quinn sector including an axion-axino-saxion supermultiplet in either the SUSY KSVZ or SUSY DFSZ models and with/without saxion decays to axions/axinos. We show allowed ranges of PQ breaking scale f_a for various cases which are generated by solving the necessary coupled Boltzmann equations. We also present results for a model with radiatively-driven naturalness but with a wino-like LSP.

KEYWORDS: [axions](#), [dark matter](#), [winos](#), [DFSZ](#), [KSVZ](#), [supersymmetry](#), [WIMPs](#).

1. Introduction

Supersymmetric models with anomaly-mediated SUSY breaking [1] (AMSB) provided a strong *raison d'être* for considering the case of a wino-like lightest SUSY particle, or LSP. Originally, such models were built with a “sequestered”– rather than a hidden– SUSY breaking sector. The sequestered sector could be located on a brane which was separated from the visible sector brane in an extra dimensional space-time. In such a case, tree level supergravity contributions to soft SUSY breaking terms were absent and the dominant contribution to soft terms came from the superconformal anomaly. Since the soft terms were all of order $m_{\text{soft}} \sim m_{3/2}/(16\pi^2)$, then values of gravitino mass $m_{3/2} \sim 30 - 100$ TeV were required to generate a weak-scale sparticle mass spectrum. The weak-scale gaugino masses were expected to occur in the ratio $M_1 : M_2 : M_3 \sim 3 : 1 : 8$, resulting in a wino-like LSP as the dark matter candidate. The thermally-produced relic density of a wino-like LSP is typically [2, 3]

$$\Omega_{\tilde{W}}^{\text{TP}} h^2 \sim 0.12 (M_2/2.5 \text{ TeV})^2. \quad (1.1)$$

The measured dark matter abundance $\Omega_{\text{CDM}} h^2 = 0.12$ is then saturated for a wino of mass $m_{\tilde{W}_1} \simeq M_2 \sim 2.5$ TeV. For lighter winos, non-thermal production mechanisms such as WIMP production from moduli decay were invoked [4].

While the simplest AMSB models provided solutions to the SUSY flavor, CP and gravitino problems, they retain the problem of predicting tachyonic slepton masses. More recently, they may have fallen into disfavor due to the discovery [5, 6] of the Higgs boson with mass $m_h = 125.5 \pm 0.5$ GeV. In the minimal AMSB model, this value of Higgs mass requires $m_{3/2} \sim 1000$ TeV so that the sparticle mass spectrum lies in the multi-TeV region which seems to seriously compromise even the most conservative measures of naturalness [7, 8].

Even well-before the Higgs discovery, related models with a wino-like LSP were emerging. These include

- PeV SUSY [2, 9],
- split SUSY [10, 11, 12],
- G2MSSM [13],
- models with strong moduli stabilization [14],
- pure gravity mediation [15, 16] and
- spread SUSY [17, 18].

These models differ from the original mAMSB model in that they predict a split spectrum with scalars ranging from 25 TeV all the way to $\sim 10^8$ TeV– well beyond the reach of collider experiments. In contrast, the gauginos typically lie in the 0.1 – 3 TeV region so that the lower range of values would be accessible to LHC searches. In most of these models, the gauginos adopt either the AMSB-form [9, 15] or a mixed anomaly plus loop contribution form [13, 17, 18] which also typically gives rise to a wino-like LSP.

The SUSY μ parameter is variable between these several models and may be as small as ~ 1 TeV [13, 16] or as high as hundreds of TeV [15]. While the predicted thermal abundance of wino-like WIMPs saturates the measured value for a wino mass of ~ 2.5 TeV (so the gaugino spectrum would be well beyond reach of LHC), for lower M_2 values a thermal underabundance of WIMPs is expected and some non-thermal DM production mechanism is needed. Usually, this has involved some form of moduli production and decay [4, 19, 20, 21] (for recent reviews, see Ref’s [22, 23]).

In the present paper, we instead look at non-thermal wino production from the Peccei-Quinn (PQ) sector.¹ By invoking a PQ sector in supersymmetric models [25] the axion supermultiplet also contains an R -parity-even spin-0 saxion s and an R -parity-odd spin-1/2 axino \tilde{a} . This approach has several advantages:

- a PQ sector seems necessary to solve the strong CP problem in the QCD sector [26, 27, 28],
- invoking PQ charges for Higgs multiplets offers a means to forbid the appearance of a Planck scale μ term while re-generating a weak-scale μ term (solution to the SUSY μ problem) [29],
- while the presence of the PQ sector can act to augment the wino abundance— for instance by axino and/or saxion decays— the axion abundance can always be adjusted to make up any remaining DM abundance which may be needed.

To explore this situation, we will adopt a benchmark model which encapsulates the dark matter physics expected in the above list of models. This benchmark point— labelled as CSB for “charged SUSY breaking” [9]— contains scalar masses around the 72 TeV region while gauginos lie in the 0.2 – 2 TeV range. The thermally-produced WIMP abundance is predicted to be $\Omega_{\tilde{W}} h^2 \sim 0.002$ — a factor ~ 60 below the measured value. Such a low thermal WIMP abundance requires additional dark matter production mechanisms to match experiment. In the case presented here, the dark matter is actually composed of both WIMPs and axions. While WIMPs can be produced thermally, they can also be produced via axino, saxion and gravitino production and decay in the early universe. In addition, saxions produced via coherent oscillations (CO) can inject late-time entropy into the early universe, thus diluting any relics already present. Axions can be produced as usual via CO [30, 31], but can also be produced thermally and via saxion decay.

While the models listed above are motivated by a variety of theoretical and phenomenological considerations, we note that collectively the entire set is highly fine-tuned in the electroweak sector, since the weak scale values of $m_{H_u}^2$ and μ^2 would have to be adjusted to very high precision to gain a Z mass of just 91.2 GeV. Thus, for contrast, we also examine a SUSY model with radiatively-driven naturalness [32] but with a wino-like LSP [33] with fine-tuning at just the 10% level (labelled as RNSw).

In Sec. 2, we briefly review a variety of models with split spectra and a wino-like LSP. We also present a SUSY model with radiatively-driven naturalness and a wino-like LSP

¹An earlier look at non-thermal production of winos in AMSB models was given in Ref. [24].

for comparison. In Sec. 3, we briefly review our coupled-Boltzmann equation evaluation of mixed axion/wino dark matter (more details can be found in Ref. [34]). In Sec. 4, we present the results of our coupled Boltzmann computation of the mixed axion/wino dark matter abundance in the CSB and RNSw benchmark models. In Sec. 5, we expand our two benchmark points to model lines to examine how our results depend on the SUSY mass spectrum. Our overall conclusions and a summary plot are given in Sec. 6.

2. Survey of some models with a wino-like LSP

2.1 PeV SUSY

In Ref. [2, 9], it is argued that the PeV scale (with $m(\text{scalars}) \sim m_{3/2} \sim 1 \text{ PeV} = 1000 \text{ TeV}$) is motivated by considerations of wino dark matter and neutrino mass while providing a decoupling solution [35] to the SUSY flavor, CP, proton decay and gravitino/moduli problems. This model invoked “charged SUSY breaking” (CSB) where the hidden sector superfield S is charged under some unspecified symmetry. In such a case, the scalars gain masses via

$$\int d^2\theta d^2\bar{\theta} \frac{S^\dagger S}{M_P^2} \Phi_i^\dagger \Phi_i \Rightarrow \frac{F_S^\dagger F_S}{M_P^2} \phi_i^* \phi_i \quad (2.1)$$

while gaugino masses, usually obtained via gravity-mediation as

$$\int d^2\theta \frac{S}{M_P} WW \Rightarrow \frac{F_s}{M_P} \lambda\lambda, \quad (2.2)$$

are now forbidden. Then the dominant contribution to gaugino masses comes from AMSB:

$$M_1 = \frac{33}{5} \frac{g_1^2}{16\pi^2} m_{3/2} \sim m_{3/2}/120, \quad (2.3)$$

$$M_2 = \frac{g_2^2}{16\pi^2} m_{3/2} \sim m_{3/2}/360, \quad (2.4)$$

$$M_3 = -3 \frac{g_3^2}{16\pi^2} m_{3/2} \sim -m_{3/2}/40. \quad (2.5)$$

$$(2.6)$$

Saturating the measured dark matter abundance with thermally-produced winos requires $m_{\tilde{W}} \sim M_2 \sim 2.5 \text{ TeV}$ which in turn requires the gravitino and scalar masses to occur at the $\sim 1000 \text{ TeV}$ (or 1 PeV) level. The author remains agnostic as to the magnitude of μ , although $\mu \gg M_2$ is expected.

2.2 Split SUSY

In Split SUSY [10, 11, 12, 36, 37], SUSY is still required for gauge coupling unification and for a dark matter candidate, but naturalness is eschewed in favor of a multi-verse solution to the gauge hierarchy problem. In such a case, matter scalars can exist with masses typically at some intermediate scale $m_{\tilde{q}, \tilde{\ell}} \sim 10^8 \text{ TeV}$ while SUSY fermions (gauginos and higgsinos) are protected by chiral symmetry and can be much lighter. Split SUSY can

be realized under charged SUSY breaking as in PeV-SUSY or via Scherk-Schwartz SUSY breaking in extra dimensions [10]. Here, one might expect

$$m(\text{gauginos}) \sim m(\text{higgsinos}) \ll m(\text{scalars}) \quad (2.7)$$

where the authors remain agnostic concerning whether the wino or bino might be lighter. Typically, binos should overproduce dark matter so that a wino/higgsino admixture might be expected.

2.3 G2MSSM

In string/M-theory models which are compactified on a manifold of G_2 holonomy [13], one expects a gravitino mass $m_{3/2} \sim 25 - 100$ TeV along with a cosmologically relevant moduli field with similar mass [38]. The matter scalar masses are of order $\sim m_{3/2}$ but gaugino masses can be much lighter. Typically, a wino LSP is to be preferred [20]. The superpotential μ term is generated with value ~ 1 TeV so that these models tend to be more electroweak-natural than split SUSY.

2.4 Models with strong moduli stabilization (Kallosh-Linde or KL)

In string theory, an outstanding problem exists in the need for vacuum stabilization of moduli fields. In the KKLT construction [39], one constructs a stable supersymmetric anti-deSitter vacuum, but then uplifts to a deSitter vacuum via SUSY breaking. In KKLT, the volume modulus mass m_σ is expected to be comparable to the gravitino mass $m_{3/2}$. These models give rise to soft SUSY breaking terms characterized by comparable moduli- and anomaly-mediated contributions [40]. However, these models suffer from vacuum destabilization during inflation unless the Hubble constant $H < m_{3/2}$. Such inflationary models, while possible, are often unwieldy and inelegant [14].

An alternative approach known as strong vacuum stabilization invokes instead a race-track superpotential for the volume modulus, leading to a far heavier modulus mass $m_\sigma \sim 10^{15}$ GeV and allowing for vacuum stability in models of chaotic inflation [14]. In this Kallosh-Linde (KL) case [41], the soft SUSY breaking scalar masses are comparable to $m_{3/2}$, but the gaugino and trilinear soft terms are suppressed by a factor of $m_{3/2}/m_\sigma$. The dominant contribution to gaugino masses comes from anomaly-mediation. Requiring a wino LSP without too much relic density then fixes $m_{3/2} \lesssim 1000$ TeV. Thus, one gains a model of split SUSY with PeV-scale scalar masses but with TeV-scale gauginos with an AMSB mass pattern. The μ parameter is also expected to be $\sim m_{3/2}$ [42] so a high degree of electroweak fine-tuning is needed.

2.5 Pure gravity-mediation

In pure gravity mediation (PGM) models [15], it is assumed that matter scalar masses are developed at tree level and so have masses $m_{\tilde{q}, \tilde{\ell}, H} \sim m_{3/2} \sim 1000$ TeV while gaugino masses are suppressed since no SUSY breaking fields are assumed to be singlets under any symmetries. The gaugino masses arise via anomaly mediation so the wino is expected to

be the LSP. The μ term and SUSY breaking bilinear B are also expected to be at the $m_{3/2}$ scale leading to

$$m_{\tilde{g},\tilde{b},\tilde{W}} \ll m_{\tilde{q},\tilde{\ell},H,\tilde{h}} \sim 100 \text{ TeV} \quad (\text{PGM}) \quad (2.8)$$

although a recent incarnation also allows for light higgsinos [16].

2.6 Spread SUSY

In Spread SUSY [17, 18], additional spatial dimensions are assumed so that the 4-d reduced Planck scale M_P is enhanced by a volume factor over the fundamental scale M_* . Then, if the hidden sector SUSY breaking field X is charged under some symmetry, gaugino masses are generated only via anomaly- mediation while scalar masses are generated via gravity-mediation. One expects a mildly split- or spread- SUSY spectrum characterized by

$$m_{\tilde{W},\tilde{b},\tilde{g}} \ll m_{3/2} \sim m_{\tilde{h}} \ll m_{\tilde{q},\tilde{\ell},H} \quad (2.9)$$

where the wino is the LSP with sub-TeV masses and the matter scalar masses may lie in the $10^2 - 10^3$ TeV range while the higgsinos are intermediate between these two.

2.7 Natural SUSY with wino-like LSP

In SUSY with radiatively-driven naturalness [32], the W, Z, h mass scale arises naturally due to a supersymmetric μ parameter with $\mu \sim 100 - 300$ GeV (the closer to m_Z the better) while $m_{H_u}^2$ is driven radiatively to small rather than large values. The TeV-scale top squark masses are highly mixed which uplifts m_h to ~ 125 GeV whilst suppressing radiative corrections to the scalar potential which influence the values of $m_{h,Z}$. While one expects a higgsino-like LSP under conditions of gaugino mass universality, models with non-universal gaugino masses allow for a bino-like or wino-like LSP without sacrificing naturalness [33]. Mixed axion-higgsino dark matter has been previously calculated in Ref's [43, 44, 34] while the mainly bino-like LSP case is largely excluded due to overproduction of WIMPs [43, 34]. Here, we consider the wino-like LSP case which typically yields a thermally-produced wino abundance of $\Omega_{\tilde{W}} h^2 \sim 0.001$ for winos with $m_{\tilde{W}} \sim 100 - 200$ GeV (at least an order-of-magnitude lower than expectations for a similarly massive higgsino LSP).

2.8 Two benchmark points

In order to compute the mixed axion/wino dark matter relic abundance in the SUSY axion models, we must specify both the PQ and the MSSM parameters. On the MSSM side, we adopt two SUSY benchmark models for illustration.

The first has been listed as benchmark CSB since it occurs in the rather simple and elegant charged SUSY breaking model of Ref. [9]. It is rather similar to the Kallosh-Linde [14] benchmark from the study of Ref. [45]. We take the CSB benchmark to be illustrative of the large class of models with multi-TeV scalars but with sub-TeV gauginos with a wino as LSP. The CSB benchmark model is listed in Table 1. We generate the SUSY model spectra with Isajet 7.83 [46].

	CSB	RNSw
m_0	72000	5000
M_1	1320	700
M_2	200	175
M_3	-600	700
A_0	0	-8000
$\tan \beta$	10	10
μ	3000	200
m_A	72000	1000
m_h	126.0	124.3
$m_{\tilde{g}}$	1924	1810
$m_{\tilde{u}_L}$	71830	5101
$m_{\tilde{t}_1}$	47760	1478
$m_{\tilde{Z}_2}$	635.9	211.8
$m_{\tilde{Z}_1}$	203.2	114.2
Δ_{EW}	22830	10.78
$\Omega_{\tilde{Z}_1}^{\text{std}} h^2$	0.0020	0.0015
$\sigma^{\text{SI}}(\tilde{Z}_1 p)$ pb	6.2×10^{-12}	4.3×10^{-8}
$\sigma^{\text{SD}}(\tilde{Z}_1 p)$ pb	1.4×10^{-8}	9.0×10^{-4}
$\langle \sigma v \rangle _{v=0}$ cm ³ /s	1.7×10^{-24}	1.7×10^{-24}

Table 1: Masses and parameters in GeV units for two benchmark points computed with Isajet 7.83 and using $m_t = 173.2$ GeV.

Along with the CSB benchmark, we adopt a natural SUSY benchmark with a wino as LSP. It is taken from Ref. [33] and denoted as RNSw (radiatively-driven natural SUSY with a wino LSP).

3. Brief review of coupled Boltzmann calculation

To accurately estimate the mixed axion/neutralino dark matter production rate in the early universe, it is necessary to evaluate the coupled Boltzmann equations which track dark matter number densities and energy densities in an intertwined manner. The exact equations used are presented in Ref. [34] and will not be repeated here. In our calculations, we use a combination of IsaReD [47] and micrOMEGAs [48] for the evaluation of the wino annihilation cross-section ($\langle \sigma v \rangle$).

The relevant equations track the following number and energy densities:

1. neutralino densities including thermal production and production via decays of heavier particles (*e.g.* axinos, saxions and gravitinos) followed by possible subsequent re-annihilation,
2. thermally-produced axinos along with axino production via heavy particle decays and diminution of axinos due to their decays,

3. thermally produced saxions along with diminution via their decays,
4. thermally-produced gravitinos [49] along with gravitino decay [50],
5. thermally-produced axions along with axion production via heavy particle decays,
6. axion production via coherent oscillations (CO) and
7. saxion production via CO along with saxion decays.
8. Along with these, we track the radiation density of SM particles.

For thermal saxion and axion production, it is reasonable to expect annihilation/production rates which are similar to axinos.

The above eight components result in 16 coupled Boltzmann equations: one for the number density and one for the energy density of each component. Together with the Friedmann equation $H = \sqrt{\rho_T/3M_P^2}$ (where ρ_T is the energy density summed over all contributions and M_P is the reduced Planck scale) the Boltzmann equations form a closed system which may be solved numerically.

For the SUSY KSVZ model, the various axino ($\tilde{a} \rightarrow g\tilde{g}$, $Z\tilde{Z}_i$ and $\gamma\tilde{Z}_i$) and saxion branching fractions ($s \rightarrow gg$, $\tilde{g}\tilde{g}$) can be found in Ref's [51, 52]. In addition, the model-dependent decays $s \rightarrow aa$, $\tilde{a}\tilde{a}$ are effectively parameterized [59] by $\xi = \sum_i q_i^3 v_i^2 / v_{PQ}^2$ where q_i are the charge assignments of PQ multiplets and v_i are their vevs after PQ symmetry breaking and $v_{PQ} = \sqrt{\sum_i v_i^2 q_i^2}$. We will take $\xi = 0$ or 1 which effectively turns off or on saxion decays to axinos/axions [43]. The decay $s \rightarrow \tilde{a}\tilde{a}$ augments the LSP abundance whilst the decay $s \rightarrow aa$ leads to dark radiation parameterized by the effective number of extra neutrinos present in the early universe ΔN_{eff} . The Planck Collaboration reported $N_{\text{eff}} = 3.52_{-0.45}^{+0.48}$ by the combined data (95%; Planck+WP+highL+ H_0 +BAO) [53].² We require the upper bound $\Delta N_{\text{eff}} < 1$ as a reference value lest too much dark radiation is produced. Excluded points with $\Delta N_{\text{eff}} > 1$ are color-coded in our results.

For the SUSY DFSZ model, axino and saxion decay rates are very different from the KSVZ case. While in the KSVZ model axino and saxion decay primarily to gauge bosons and gauginos, in SUSY DFSZ then typically $\tilde{a} \rightarrow \tilde{Z}_i \phi$ (where $\phi = h, H, A$), $\tilde{Z}_i Z$, $\tilde{W}_j W$ and $\tilde{W}_j^\mp H^\pm$ and $s \rightarrow$ pairs of Higgs bosons, vector bosons and electroweak-ino pairs. Complete formulae for the DFSZ decay rates are found in Ref. [44].

The thermal production rates for SUSY KSVZ (which are proportional to T_R) are found in Ref's [55] while thermal production rates for SUSY DFSZ (which are mostly independent of T_R) are obtained from Ref's [56]. We include production of particles via both decays and inverse decays [34]: the latter effects are important in SUSY DFSZ where saxions and axinos are maximally produced at $T \sim m(\text{particle})$ which leads to a freeze-in effect [57] which manifests itself essentially as delayed saxion/axino decays.

An example of the evolution of various energy densities ρ_i vs. the cosmic scale factor R/R_0 is shown in Fig. 1 for the SUSY DFSZ model. R_0 is taken to be the scale factor at

²As this paper was being finalized, this value was updated [54] to $N_{\text{eff}} = 3.15 \pm 0.23$.

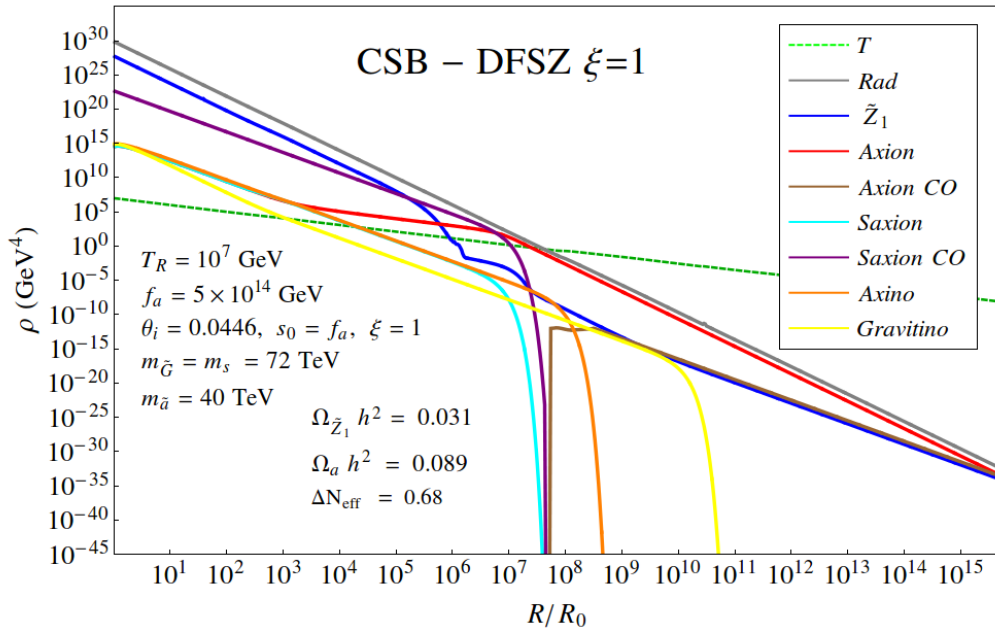


Figure 1: Evolution of various energy densities vs. scale factor R/R_0 for the CSB benchmark case in SUSY DFSZ with $\xi = 1$ and other parameters as indicated in the figure.

the end of reheating ($T = T_R$). In the figure, $f_a = 5 \times 10^{14}$ GeV while $m_s = m_{3/2} = 72$ TeV for the CSB benchmark point. We also take $m_{\tilde{a}} = 40$ TeV and $\xi = 1$ so that saxion decay to axions is turned on. At $R/R_0 = 1$, the universe is indeed radiation dominated (gray curve) while including a thermal population of WIMPs, saxions, axions, axinos and gravitinos. It also includes a CO-component of saxions. As R/R_0 increases (decreasing temperature as denoted by the green dashed line), the oscillating saxion field begins to decay—mainly via $s \rightarrow aa$ —so that the population of thermal/decay-produced axions (red curve) increases beyond its otherwise thermal trajectory around and below $R/R_0 \sim 10^4$. The neutralino abundance (dark blue) begins to freeze-out around $R/R_0 \sim 10^5$, but then is augmented by decaying CO saxions and also by axinos (which decay slightly after saxions). Decaying gravitinos add, but only marginally, to the neutralino abundance around $R/R_0 \sim 10^{10}$. At $R/R_0 \sim 10^8$, the axion mass turns on and the axion field begins to oscillate as non-relativistic matter (brown curve). Also, at $R/R_0 \sim 10^9$, the neutralinos become non-relativistic. Together, the combined neutralino-axion CDM ultimately dominates the universe at around $R/R_0 \sim 10^{16}$. The ultimate dark matter density is composed of $\sim 25\%$ wino-like WIMPs and $\sim 75\%$ cold axions with a modest-but-not-yet-excluded contribution of relativistic axions ($\Delta N_{\text{eff}} = 0.68$) as dark radiation.

4. Mixed axion-wino dark matter

In the following subsections, we compute the neutralino and axion relic abundances for

the two benchmark points through numerical integration of the Boltzmann equations as discussed in Sec. 3. To gain more general results, we will scan over the PQ scale f_a and the axino mass which we take to be bounded by $m_{3/2}$:

$$\begin{aligned} 10^9 \text{ GeV} &< f_a < 10^{16} \text{ GeV}, \\ 0.4 \text{ TeV} &< m_{\tilde{a}} < m_{3/2}, \end{aligned} \tag{4.1}$$

with m_s fixed as $m_s = m_{3/2}$. In many supergravity models, saxion mass is generated by the same operators as those for the MSSM scalars while axino mass is highly model dependent and can be much smaller than $m_{3/2}$ [58, 59]. For this reason, we consider the above parameter range for our general analyses.

For simplicity, we will fix the initial saxion field strength, which sets the amplitude of coherent saxion oscillations, to $s_i = f_a$ ($\theta_s \equiv s_i/f_a = 1$). In addition— for points which are DM-allowed ($\Omega_{\tilde{Z}_1} h^2 < 0.12$) and obey BBN and dark radiation constraints— the initial axion mis-alignment angle θ_i is set to the required value such that $\Omega_{\tilde{Z}_1} h^2 + \Omega_a h^2 = 0.12$. In the SUSY DFSZ case, unlike the SUSY KSVZ model, the bulk of our results do not depend strongly on the re-heat temperature (T_R) since the axion, axino and saxion TP rates are largely independent of this quantity. Nonetheless, the gravitino thermal abundance is proportional to T_R and since gravitinos are long-lived they may affect BBN or WIMP abundance constraints if T_R is sufficiently large. In order to avoid the BBN constraints on gravitinos, we choose $T_R = 10^7$ GeV, which results in a sufficiently small (would-be) gravitino abundance. As a result, gravitinos typically do not contribute significantly to the neutralino abundance, as discussed above.

For each of the CSB and RNSw benchmark points, we consider two different cases: $\xi = 0$ (saxion decay to axions/axinos turned off) and $\xi = 1$ (saxion decay to axions/axinos turned on). We adopt a KSVZ model with $SU(2)_L$ singlet heavy quark states so that the axion superfield only has interactions with $SU(3)_c$ and $U(1)_Y$ gauge superfields. We discuss the case of $SU(2)_L$ doublet heavy quark states in Sec. 6 for completeness.

4.1 CSB benchmark in SUSY KSVZ

4.1.1 $\xi = 0$ case

In this section, we will examine the CSB benchmark in the SUSY KSVZ case. We start with the case where saxion decays into axinos and axions are turned off ($\xi = 0$). Results for this benchmark are shown in Fig. 2, where we plot $\Omega_{\tilde{Z}_1} h^2$ (blue points) and $\Omega_a h^2$ (green points) vs. f_a for the scan over parameters defined in Eq. (4.1). In the figure, red points violate BBN bounds on late-decaying neutral relics [60] while otherwise the points are BBN safe. We also show the measured abundance of CDM by the solid horizontal line. Points above this line are excluded by overproduction of dark matter while points below the line are allowed. The dashed horizontal grey line denotes the 50% CDM abundance so that blue points above this line have WIMP-dominated CDM while green points above this line have axion-dominated CDM.

In Fig. 2, one can see that there are three branches of the neutralino CDM density for $f_a \lesssim 10^{15}$ GeV. These branches reflect three regions of axino mass. The uppermost

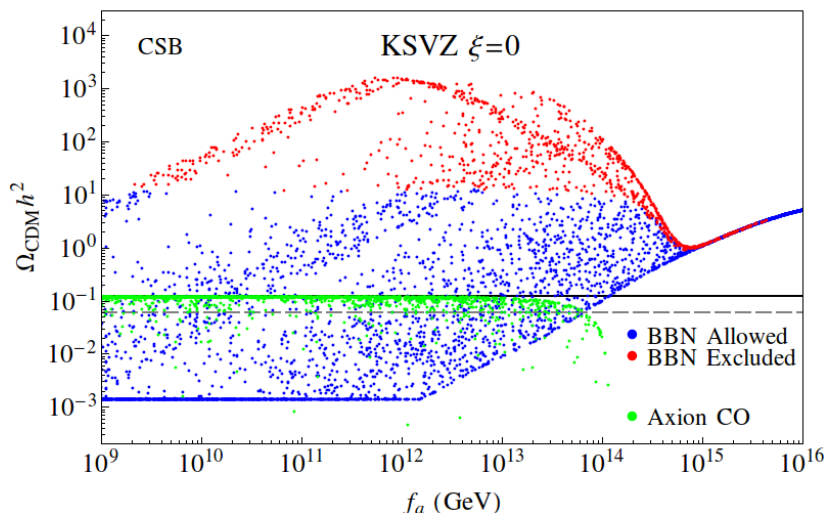


Figure 2: The wino-like WIMP (blue) and axion (green) relic densities from a scan over SUSY KSVZ parameter space for the CSB benchmark case with $\xi = 0$. The grey dashed line shows the points where DM consists of 50% axions and 50% neutralinos.

branch corresponds to the case of $m_{\tilde{a}} < m_{\tilde{Z}_2}$. In this case, axinos decay only into \tilde{Z}_1 plus SM particles. Since the axion sector does not have a direct coupling to a $SU(2)_L$ gauge supermultiplet, axino decays into \tilde{Z}_1 (mostly wino-like) happen only through the bino-wino mixing, which is very tiny in the MSSM. Therefore, for this branch the axino decay occurs well-after the neutralino freeze-out, enhancing the neutralino abundance well above the measured CDM density for all values of f_a . Moreover— for $f_a \gtrsim 10^{10}$ GeV— BBN constrains the model due to the long-lived axino.

The middle branch corresponds to $m_{\tilde{Z}_2} < m_{\tilde{a}} < m_{\tilde{g}}$. In this region axinos can decay directly into \tilde{Z}_2 . Since \tilde{Z}_2 is mostly bino-like and axinos directly couple to \tilde{B} through the $U(1)_Y$ anomalous coupling, their life-time is much shorter than in the $m_{\tilde{a}} < m_{\tilde{Z}_2}$ case. Although the axinos decay after neutralino freeze-out for all f_a , the neutralino density still is smaller than the observed CDM density for $f_a \lesssim 5 \times 10^{10}$ GeV. Hence, both axion-dominated or neutralino-dominated dark matter scenarios are possible in this region. For $f_a \gtrsim 5 \times 10^{12}$ GeV, all points in the $m_{\tilde{a}} < m_{\tilde{g}}$ branch are excluded by BBN.

The lowermost branch corresponds to $m_{\tilde{a}} > m_{\tilde{g}}$. In this region, axinos can decay to gluinos through the $SU(3)_c$ anomaly coupling so that the axino life-time becomes much shorter than the previous two cases. For $f_a \lesssim 10^{12}$ GeV, axinos decay before neutralino freeze-out in the bulk of this parameter region, so the neutralino CDM density takes its standard thermal value ~ 0.002 . In the case where the axino mass is close to the gluino mass, however, axinos can decay after neutralino freeze-out and augment the WIMP abundance. As f_a increases, axinos more often decay after freeze-out and hence increasingly augment the neutralino relic density. By $f_a \sim 2 \times 10^{12}$ GeV, axinos always decay after freeze-out and always augment the neutralino abundance. Despite the enhancement of the neutralino abundance, there are points where the DM is axion-dominated up to

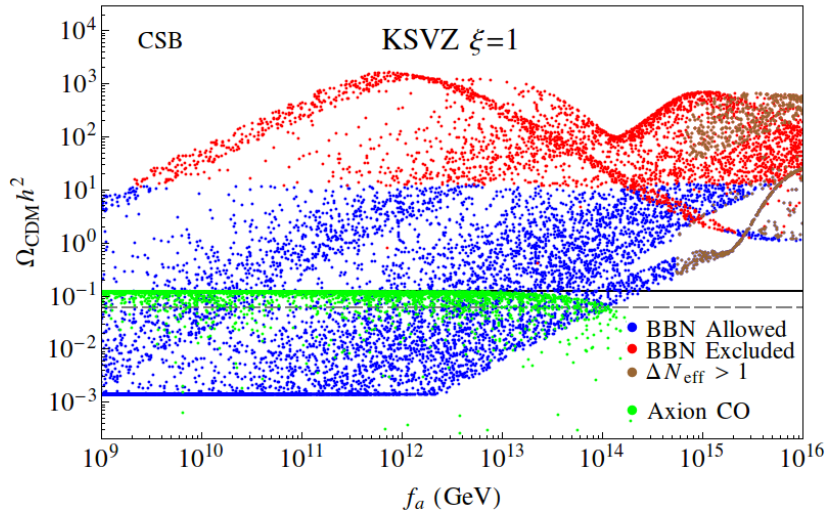


Figure 3: The wino-like WIMP and axion relic densities from a scan over SUSY KSVZ parameter space for the CSB benchmark case with $\xi = 1$. The grey dashed line shows the points where DM consists of 50% axions and 50% neutralinos.

$f_a \simeq 6 \times 10^{13}$ GeV.

For $f_a \gtrsim 10^{15}$ GeV, the contribution to the WIMP abundance is mostly from CO-produced saxion decays; these augment the abundance for larger f_a since the saxion CO production rate increases with f_a . On the other hand, the contribution from TP axinos is highly suppressed for large f_a , since the axino thermal production decreases with f_a . Once the TP axino abundance becomes negligible ($f_a \gtrsim 5 \times 10^{14}$ GeV), the LSP relic abundance becomes independent of the axino mass and all the branches discussed above collapse into a single line, as seen in Fig. 2.

4.1.2 $\xi = 1$ case

In Fig. 3, we show $\Omega_{\tilde{Z}_1, a} h^2$ vs. f_a for the same CSB benchmark point but now where saxion decays into axinos and axions are allowed: $\xi = 1$. For the lower ($f_a \lesssim 10^{14}$ GeV) range, saxion decays have a smaller impact on the neutralino abundance and the results are similar to the CSB/KSVZ $\xi = 0$ case. For higher f_a values, CO-produced saxions become important and since $s \rightarrow aa$ and $\tilde{a}\tilde{a}$ decays are now allowed, there is a large injection of relativistic axions. For $f_a > 4 \times 10^{14}$ GeV, we see brown points which produce too much dark radiation— $\Delta N_{\text{eff}} > 1$ — and are excluded. There is also a broad band of blue (BBN-allowed) and red (BBN-excluded) points at large $f_a \sim 10^{15}$ GeV with very high $\Omega_{\tilde{Z}_1} h^2 \sim 1 - 100$ where the additional neutralino abundance arises from $s \rightarrow \tilde{a}\tilde{a}$ decays. The lower disjoint narrow band at $f_a \gtrsim 10^{14}$ GeV and $\Omega_{\tilde{Z}_1} h^2 \sim 0.1 - 1$ occurs for points where $m_{\tilde{a}} > m_s/2$, so $s \rightarrow \tilde{a}\tilde{a}$ is kinematically forbidden.

Finally we point out that, unlike the $\xi = 0$ case, the extremely large f_a region ($f_a \gtrsim 10^{15}$ GeV) still shows a dependence on the axino mass: this is responsible for the distinct branches. Although thermal production of axinos is negligible in this regime, axi-

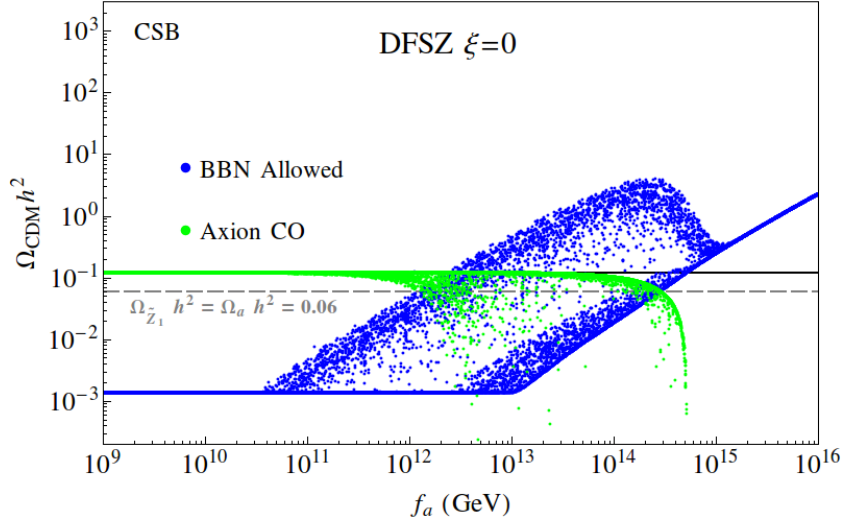


Figure 4: The wino-like WIMP and axion relic densities from a scan over SUSY DFSZ parameter space for the CSB benchmark case with $\xi = 0$. The grey dashed line shows the points where DM consists of 50% axions and 50% neutralinos.

nos are non-thermally produced from saxion decays and can influence the final neutralino abundance.

4.2 CSB benchmark in SUSY DFSZ

4.2.1 $\xi = 0$ case

In this section, we will examine the CSB benchmark in the SUSY DFSZ case. As before, we start with the $\xi = 0$ case, shown in Fig. 4. The first noteworthy point is that the large μ value enhances the saxion (axino) decay rate to Higgs (higgsinos). As a result the saxion and axino lifetimes are suppressed and the entire f_a range is BBN safe. Unlike the KSVZ case, there are two branches for neutralino CDM density, since in the DFSZ case, the axino decay is determined by the μ -term interaction. The upper branch corresponds to $m_{\tilde{a}} < m_{\tilde{Z}_3} \sim \mu$ with higgsino-like \tilde{Z}_3 . The axino decay into \tilde{Z}_1 or \tilde{Z}_2 can be through wino-higgsino or bino-higgsino mixing, so it is normally suppressed by $(m_Z/\mu)^2$. For $f_a \lesssim 3 \times 10^{10}$ GeV, axinos decay before neutralino freeze-out, and thus the neutralino density takes its standard value. For $f_a \gtrsim 3 \times 10^{10}$ GeV, axinos tends to decay after neutralino freeze-out so the neutralino density gradually increases as f_a increases. In most of parameter space, axions constitute the bulk of dark matter, but wino-like neutralinos can be the dominant dark matter in the region of $10^{12} \text{ GeV} \lesssim f_a \lesssim 10^{13} \text{ GeV}$. By $f_a \gtrsim 10^{13} - 10^{14}$ GeV, the neutralino density is typically larger than the measured CDM result so the parameter/model choices would be excluded.

The lower branch corresponds to $m_{\tilde{a}} > m_{\tilde{Z}_3}$. Due to its large interaction, the axino tends to decay before neutralino freeze-out for $f_a \lesssim 3 \times 10^{12}$ GeV. Therefore, the neutralino relic abundance is usually fixed at its thermally-produced value for much of the lower range of f_a . Once $f_a \gtrsim 10^{13}$ GeV, the neutralino abundance is always enhanced due to decays

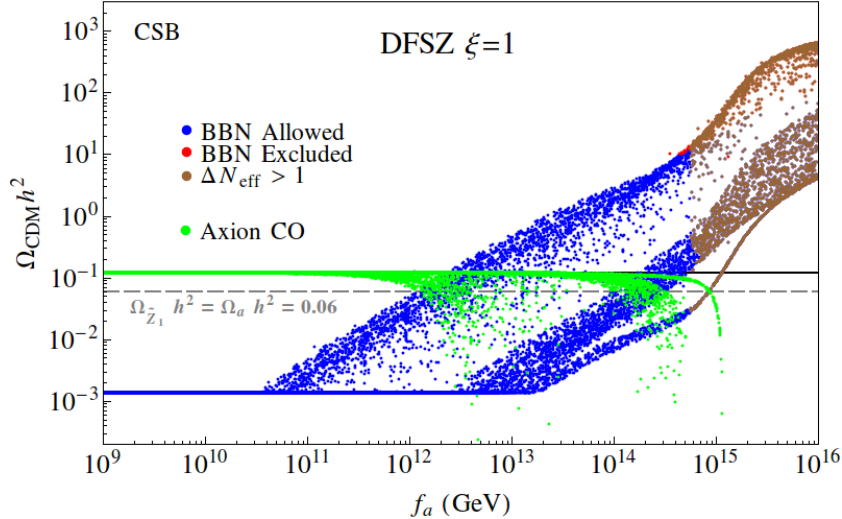


Figure 5: The wino-like WIMP and axion relic densities from a scan over SUSY DFSZ parameter space for the CSB benchmark case with $\xi = 1$. The grey dashed line shows the points where DM consists of 50% axions and 50% neutralinos.

of axinos and saxions. Still, the CDM abundance tends to be axion-dominated for $f_a \lesssim 2 \times 10^{14}$ GeV. For higher f_a there is a short interval where wino-like WIMPs can dominate the DM abundance. Finally, for $f_a \gtrsim 6 \times 10^{14}$ GeV, WIMP CDM is always overproduced. We also point out that for very large f_a values, as in the KSVZ $\xi = 0$ scenario, the thermal production of axinos is negligible hence the neutralino relic abundance becomes independent of f_a .

4.2.2 $\xi = 1$ case

For the CSB benchmark with SUSY DFSZ and $\xi = 1$, the results are shown in Fig. 5. The low f_a behavior of the plot is similar to the CSB/DFSZ case with $\xi = 0$: the CDM density is dominated by axions. For higher f_a values, where CO-produced saxions become important, the saxion lifetime is shortened by the additional contributions from $s \rightarrow aa, \tilde{a}\tilde{a}$ decays. However, most of the points for $f_a \gtrsim 5 \times 10^{14}$ GeV are forbidden due to overproduction of dark radiation. The lower blue-brown band at $f_a \sim 10^{14} - 10^{15}$ GeV occurs when $m_{\tilde{a}} > m_s/2$ so that additional WIMP production from $s \rightarrow \tilde{a}\tilde{a}$ is dis-allowed.

4.3 RNSw benchmark in SUSY KSVZ

In this subsection we examine dark matter production in the SUSY RNSw benchmark case. The RNSw benchmark model has values $m_s = m_0 \equiv m_{3/2} = 5$ TeV which is far smaller than that of the CSB benchmark so that saxions (and also axinos since we take their mass to be bounded by $m_{3/2}$) are typically much longer-lived than in the CSB case.

4.3.1 $\xi = 0$ case

In Fig. 6, we plot $\Omega_{\tilde{Z}_{1,a}} h^2$ vs. f_a for the SUSY KSVZ case using the RNSw benchmark point

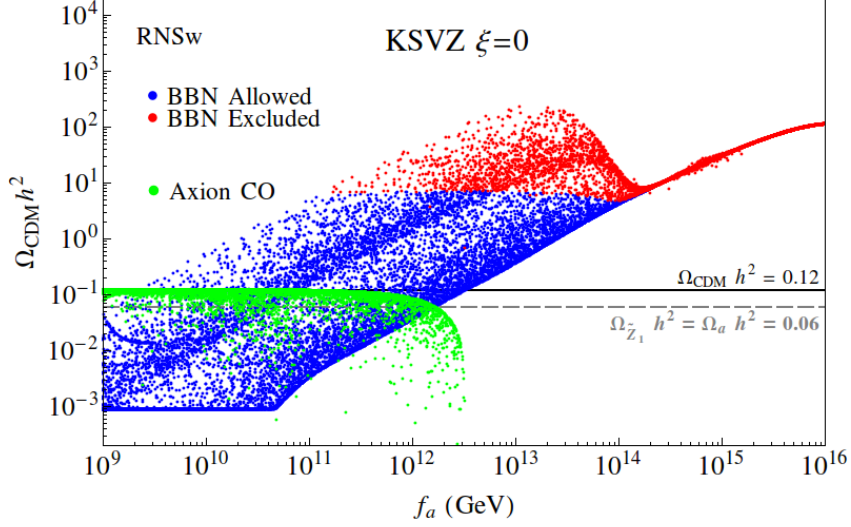


Figure 6: The wino-like WIMP and axion relic densities from a scan over SUSY KSVZ parameter space for the RNSw benchmark case with $\xi = 0$. The grey dashed line shows the points where DM consists of 50% axions and 50% neutralinos.

with $\xi = 0$. In this case, $m_{\tilde{a}}$ is always larger than $m_{\tilde{Z}_2}$, so there are only two branches for the neutralino density: $m_{\tilde{a}} < m_{\tilde{g}}$ and $m_{\tilde{a}} > m_{\tilde{g}}$. Long-lived axinos are already augmenting the neutralino relic density even at f_a values as low as 10^9 GeV. As we move to higher f_a values, the axinos and saxions are longer-lived, thus contributing even more to the WIMP abundance. For f_a values $\gtrsim 5 \times 10^{12}$ GeV, the model is already excluded due to overproduction of WIMPs. The $\Omega_{\tilde{Z}_1} h^2$ points reach even higher values as f_a increases until $f_a \sim 3 \times 10^{13}$ GeV. For 3×10^{13} GeV $\lesssim f_a \lesssim 2 \times 10^{14}$ GeV, the axino contribution decreases due to suppression of the thermal production. For $f_a \gtrsim 2 \times 10^{14}$ GeV, then CO-produced saxions decay into gluino pairs and tend to augment the WIMP abundance. However, this is inconsequential since the model already overproduces WIMP dark matter. A large BBN forbidden region occurs, but it is already in the WIMP-overproduction region so adds no further constraints.

4.3.2 $\xi = 1$ case

For the RNSw benchmark case in SUSY KSVZ with $\xi = 1$, as shown in Fig. 7, the low f_a behavior of $\Omega_{\tilde{Z}_1} h^2$ is very similar to the $\xi = 0$ case, since at low f_a saxion production is not very relevant and saxions decay well-before neutralino freeze-out. For $f_a \gtrsim 4 \times 10^{12}$ GeV, as in the $\xi = 0$ case, the model over-produces WIMPs and is excluded. At even larger values of f_a , in the DM-excluded region, the $\xi = 1$ case begins to differ from $\xi = 0$. An additional branch of $\Omega_{\tilde{Z}_1} h^2$ appears: the lowermost branch swings downward due to the suppressed axino and saxion TP as in the $\xi = 0$ case, but never reaches the DM-allowed line. It is nonetheless also excluded by overproduction of dark radiation. The upper (also excluded) two branches occur where $m_s > 2m_{\tilde{a}}$ so that CO-production of saxions keeps increasing the WIMP abundance. This region is also excluded by the BBN constraint from

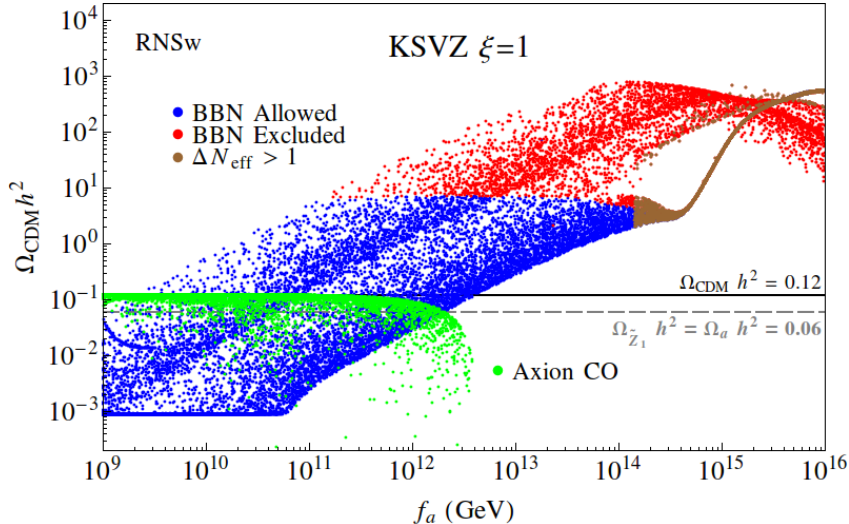


Figure 7: The wino-like WIMP and axion relic densities from a scan over SUSY KSVZ parameter space for the RNSw benchmark case with $\xi = 1$. The grey dashed line shows the points where DM consists of 50% axions and 50% neutralinos.

late-decaying saxions followed by axino cascade decays.

4.4 RNSw benchmark in SUSY DFSZ

In this subsection, we examine the RNSw benchmark model in the SUSY DFSZ model. Since $\mu(\text{RNSw}) \ll \mu(\text{CSB})$, saxions in the RNSw/DFSZ case will tend to be longer lived.

4.4.1 $\xi = 0$ case

In Fig. 8 we show RNSw in the SUSY DFSZ case with $\xi = 0$. In this case, $m_{\tilde{a}}$ is always larger than μ , so there is no region corresponding to the upper branch in Fig. 4. For low f_a , in contrast to RNSw in the SUSY KSVZ case, the axino lifetime is smaller and the WIMP abundance remains at its thermally-produced value for $f_a \lesssim 5 \times 10^{10}$ GeV. For higher f_a values, the WIMP abundance is augmented by axino and saxion decays after freeze-out. Ultimately, the model over-produces WIMPs for $f_a \gtrsim 10^{13}$ GeV. The model tends to be axion-dominated for $f_a \lesssim 6 \times 10^{12}$ GeV and WIMP dominated for a narrow range of f_a just beyond this value until WIMP overproduction is reached and the model becomes excluded. This is in contrast to the CSB benchmark with DFSZ and $\xi = 0$, where the allowed region extends to $f_a \sim 5 \times 10^{14}$ GeV since saxions and axinos are shorter-lived due to much larger masses and stronger interactions ($\mu(\text{RNSw}) \ll \mu(\text{CSB})$).

4.4.2 $\xi = 1$ case

In Fig. 9 we show results for the RNSw benchmark in SUSY DFSZ with $\xi = 1$. While the low f_a behavior is similar to the results from the $\xi = 0$ case, the high f_a behavior is different. The decays $s \rightarrow aa$ and $s \rightarrow \tilde{a}\tilde{a}$ allow the saxion to decay more quickly than in the $\xi = 0$ case for a common value of f_a . Thus, the DM-allowed region extends to larger f_a

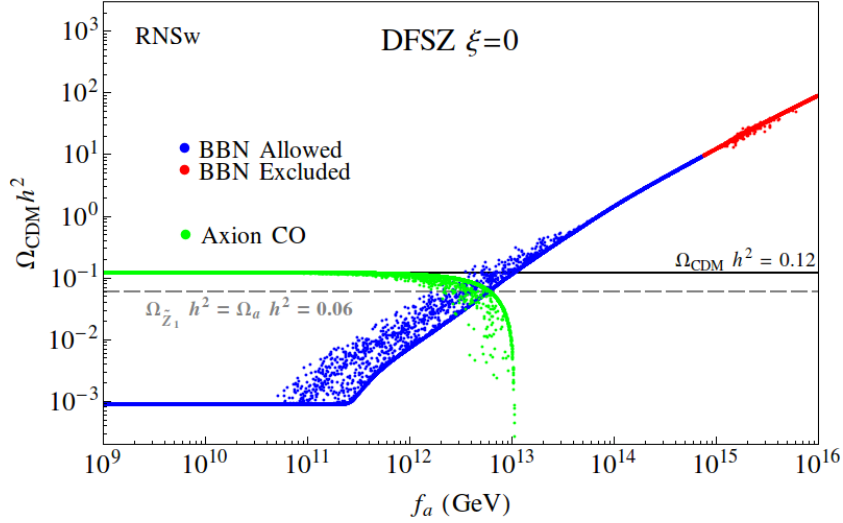


Figure 8: The wino-like WIMP and axion relic densities from a scan over SUSY DFSZ parameter space for the RNSw benchmark case with $\xi = 0$. The grey dashed line shows the points where DM consists of 50% axions and 50% neutralinos.

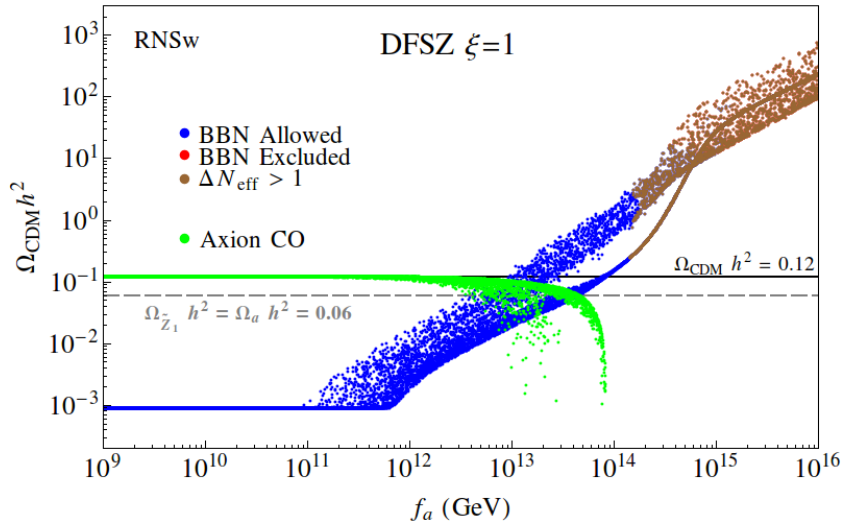


Figure 9: The wino-like WIMP and axion relic densities from a scan over SUSY DFSZ parameter space for the RNSw benchmark case with $\xi = 1$. The grey dashed line shows the points where DM consists of 50% axions and 50% neutralinos.

values: in this case up to $f_a \sim 10^{14}$ GeV. For these high f_a values, the relic density band again splits into two branches: one with heavy axinos (lower-branch), where $s \rightarrow \tilde{a}\tilde{a}$ is closed, and one with light axinos (upper branch), where $s \rightarrow \tilde{a}\tilde{a}$ is open, thus augmenting the WIMP abundance. The points with $f_a \gtrsim 2 \times 10^{14}$ GeV tend to be doubly-excluded by overproduction of WIMPs and by overproduction of dark radiation.

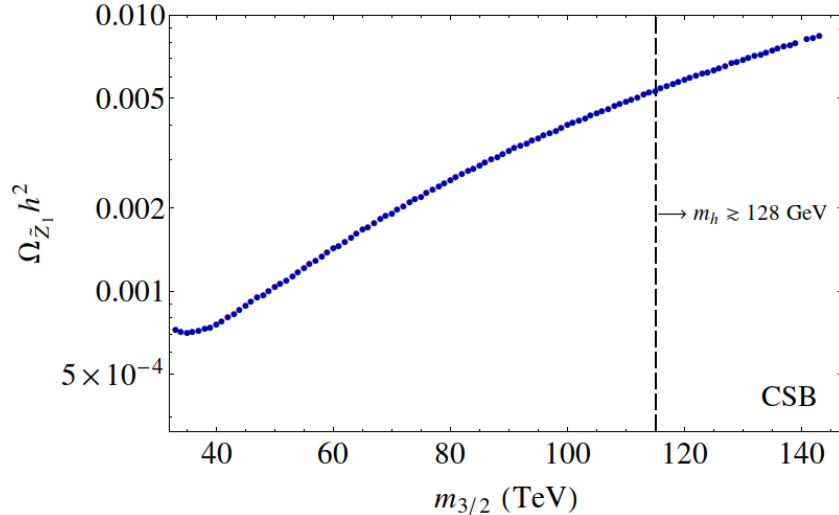


Figure 10: Plot of thermally-produced neutralino abundance $\Omega_{\tilde{Z}_1} h^2$ vs. $m_{3/2}$ along the CSB model line with $\tan\beta = 10$ and $\mu = 3$ TeV.

5. Dependence of mixed axion-wino abundance on sparticle mass spectra

In the previous sections we have investigated the DM-allowed range of f_a for two SUSY benchmark models with wino-like LSPs, f_a and $m_{\tilde{a}}$ as free parameters and $m_s = m_0$. In this section, we investigate how our results might change as a function of the MSSM spectrum. To explore this issue, we extend our two benchmark points into model lines in the MSSM sector. For brevity, we consider here only the DFSZ model– which provides a solution to the SUSY μ problem– to see the impacts of axino/saxion production/decays on the CDM density. Actually, even in the presence of late-decaying axinos and saxions, the most important factor that determines the WIMP abundance is the WIMP-WIMP annihilation cross section since the augmented density is determined mainly by annihilation cross section evaluated at the heavy particle decay temperature: this is the case of so-called WIMP re-annihilation after non-thermal WIMP production from heavy particle decay [51]. For this reason, the behavior of our plots is similar for both DFSZ and KSVZ models, and so we will show only the DFSZ case and then briefly comment on the KSVZ case.

5.1 CSB model line

For the CSB benchmark, we will now allow $m_{3/2}$ to vary while keeping $\tan\beta$ fixed at 10 with $\mu = 3$ TeV and $m_A = m_{3/2}$. For the CSB model-line, we require $m_{3/2} \gtrsim 32$ TeV so the mass of the lightest wino-like chargino is always above the limit $m_{\tilde{W}_1} \gtrsim 91.9$ GeV established from LEP2 searches. The upper limit on $m_{3/2}$ occurs at ~ 115 TeV where the predicted value of m_h climbs above 128 GeV. Here, we allow for an expected theory error in the Isasugra calculation of m_h at about ± 2.5 GeV.

We show the thermally-produced neutralino abundance for the CSB model line in Fig. 10. Here, we see that $\Omega_{\tilde{Z}_1}^{\text{TP}} h^2$ ranges from around 0.0007 at the lower limit to about

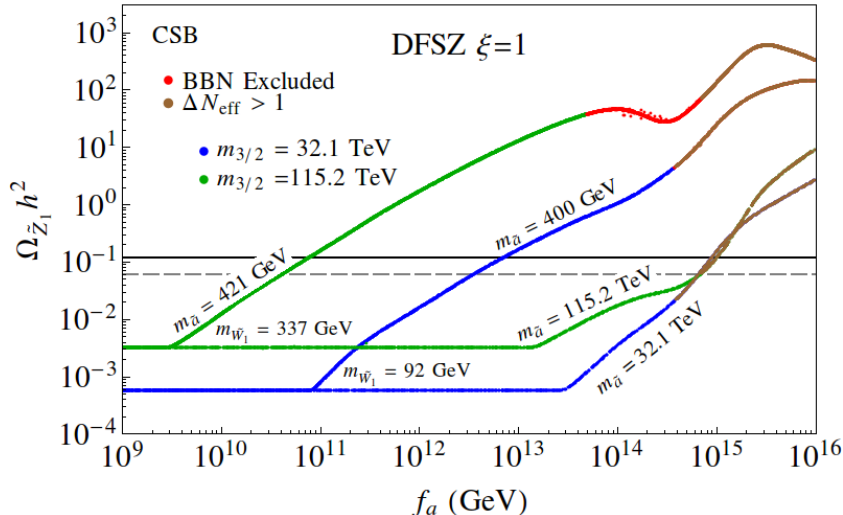


Figure 11: Plot of thermally- and non-thermally-produced neutralino abundance $\Omega_{\tilde{Z}_1} h^2$ vs. f_a along the CSB model line in the DFSZ $\xi = 1$ case for a light ($m_{3/2} = 32$ TeV, blue envelope) and heavy ($m_{3/2} = 115$ TeV, green envelope) CSB mass spectrum where $m_{\tilde{a}}$ ranges from 400 GeV up to $m_{3/2}$.

0.005 at the upper limit as compared to 0.002 for the CSB benchmark. Roughly speaking, the thermally-produced wino abundance will provide either more or less room in general for non-thermally produced winos and axinos.

In Fig. 11, we show the value of $\Omega_{\tilde{Z}_1} h^2$ which is produced from the coupled Boltzmann calculation of mixed axion-wino CDM versus f_a for the minimal and maximal values of $m_{3/2}$ which are allowed along the CSB model line. The blue curves provide the calculated envelope of values for the lower limit of $m_{3/2} \sim 32$ TeV. At low f_a , $\Omega_{\tilde{Z}_1} h^2$ lies at the TP-value ~ 0.0006 since thermally-produced axinos always decay before neutralino freeze-out. As f_a climbs above $\sim 10^{11}$ GeV, then the lighter axinos start decaying after neutralino freeze-out whilst the heavier axinos still decay before freeze-out. The region between the two blue curves shows the range of $\Omega_{\tilde{Z}_1} h^2$ which is generated for $0.4 \text{ TeV} < m_{\tilde{a}} < 32$ TeV. We see that values of f_a up to $\sim 10^{15}$ GeV are dark-matter-allowed for very heavy axinos. However, at values of $f_a \gtrsim 5 \times 10^{14}$ GeV, then too much dark radiation is produced from $s \rightarrow aa$ decays in addition to WIMP overproduction so that the parameter space is doubly-excluded.

The heavy end of the CSB model line $m_{3/2} = 115$ TeV is shown by the envelope of green curves. For the light axino with $m_{\tilde{a}} = 421$ GeV, the thermally-produced value of $\Omega_{\tilde{Z}_1} h^2 \sim 0.003$ is obtained only for the short range of $f_a \lesssim 3 \times 10^9$ GeV. For this heavy CSB spectra, the gauginos are all sufficiently heavy and thus the axino can decay only into \tilde{Z}_1 so that the axino lifetimes are much longer than that in the case for light spectra. The upper range of the green envelope comes from light axino masses where $m_{\tilde{a}} = 421$ GeV is the threshold for $\tilde{a} \rightarrow Z\tilde{Z}_1$ decay hence augmenting neutralino density at low f_a , while the lower envelope is established by the heaviest axino mass values. For the upper part

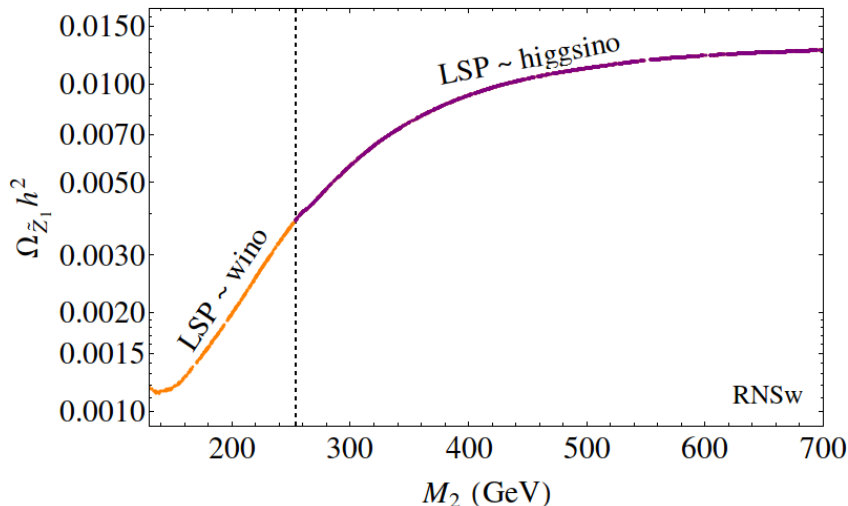


Figure 12: Plot of thermally-produced neutralino abundance $\Omega_{\tilde{Z}_1} h^2$ vs. M_2 along the RNSw model line.

of the envelope, the red points denote the on-set of BBN bounds on late decaying saxions as ruling out $f_a \gtrsim 5 \times 10^{13}$ GeV. For the lower part of the envelope, with axino masses ranging to 32 TeV, then values of f_a up to 5×10^{14} GeV are possible.

In the case of KSVZ model, the spectrum dependence is similar to the DFSZ model. For the light spectrum ($m_{3/2} = 32$ TeV), the neutralino abundance tends to be smaller due to its large annihilation cross section. For the heavy spectrum ($m_{3/2} = 115$ TeV), the cross section becomes larger, so the neutralino abundance becomes smaller. Nevertheless, the allowed range of f_a for the heavy spectrum is slightly larger than that for light spectrum since the saxion mass is larger ($m_s = m_{3/2}$) so that its decay can occur earlier.

5.2 RNSw model line

For the RNSw benchmark, we will instead allow the GUT scale $SU(2)_L$ gaugino mass M_2 to vary while keeping $m_0 = 5$ TeV, $m_{1/2} = 700$ GeV, $A_0 = -8$ TeV and $\tan\beta$ fixed at 10 with $\mu = 200$ GeV and $m_A = 1$ TeV. For the RNSw model-line, the lower limit on M_2 is again set by the limit from LEP2 searches for wino-like charginos. The upper limit on $M_2 \lesssim 250$ GeV is set from simply requiring a wino-like LSP: for higher M_2 values, the lightest neutralino becomes increasingly higgsino-like, a case which was shown in Ref's [44, 34]. The naturalness value Δ_{EW} remains fixed at around 10 since varying M_2 hardly affects it [33].

We show the thermally-produced neutralino abundance for the RNSw model line in Fig. 12. The lower range of $\Omega_{\tilde{Z}_1}^{\text{TP}} h^2$ occurs at 0.0012 for $M_2 \sim 140$ GeV. The maximal value reaches up to ~ 0.004 before entering the higgsino-like LSP region. Since the thermally-produced wino abundance increases with M_2 , the allowed enhancement from non-thermal production decreases as M_2 increases. Furthermore, since the non-thermal production (from saxion and axino decays) grows with f_a , we expect the maximum allowed value for

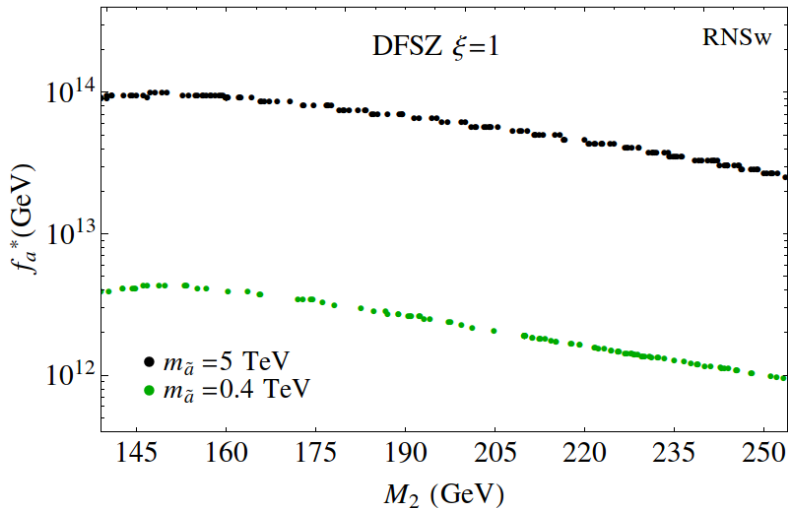


Figure 13: Plot of upper limit of f_a allowed from the RNSw model line in the DFSZ case with $\xi = 1$ versus M_2 for $m_{\tilde{a}} = 400$ GeV and $m_{\tilde{a}} = 5$ TeV.

f_a to decrease as M_2 increases. This is shown in Fig. 13, where we plot the upper limit on f_a , denoted as f_a^* , versus M_2 along the RNSw model line in the DFSZ $\xi = 1$ case. The axino mass is $m_{\tilde{a}} = 0.4$ TeV (green dots) or $m_{\tilde{a}} = 5$ TeV (black dots). The upper limit comes only from the overproduction of WIMPs in this case since violation of BBN bounds and overproduction of dark matter occurs at higher f_a in this model.

In the KSVZ model, on the other hand, axinos are longer-lived than in the DFSZ model, so the allowed range of f_a is smaller than that in the DFSZ case. As we have seen in Fig. 7, only a small region, $f_a \lesssim \mathcal{O}(10^{10})$ GeV, is allowed for $m_{\tilde{a}} \lesssim m_{\tilde{g}}$, while $f_a \lesssim \mathcal{O}(10^{12})$ GeV is allowed for $m_{\tilde{a}} = 5$ TeV.

6. Conclusion

In this paper we have examined mixed axion/wino cold dark matter production in two SUSY benchmark models with a wino as LSP. The first—labeled as CSB—is typical of a variety of models (PeV-SUSY, some split SUSY variations, KL, PGM, spread SUSY) with a thermally-underproduced wino-like WIMP abundance. The second, labeled as RNSw, is a model with radiatively-driven naturalness but with a wino-like rather than a higgsino-like LSP. Our calculation of mixed axion/wino dark matter production stands in contrast to the more commonly examined case of non-thermal WIMP production due to late decaying moduli fields [4, 19, 20]. We find it a more appealing method for augmenting the dark matter abundance since it also provides a solution to the strong CP problem and—in the case of SUSY DFSZ—provides for a solution to the SUSY μ problem.

We have presented results for the wino-like WIMP abundance and axion abundance as a function of the axion decay constant f_a and the axino mass $m_{\tilde{a}}$. In the bulk of the parameter space, WIMPs are thermally under-produced at low and intermediate f_a

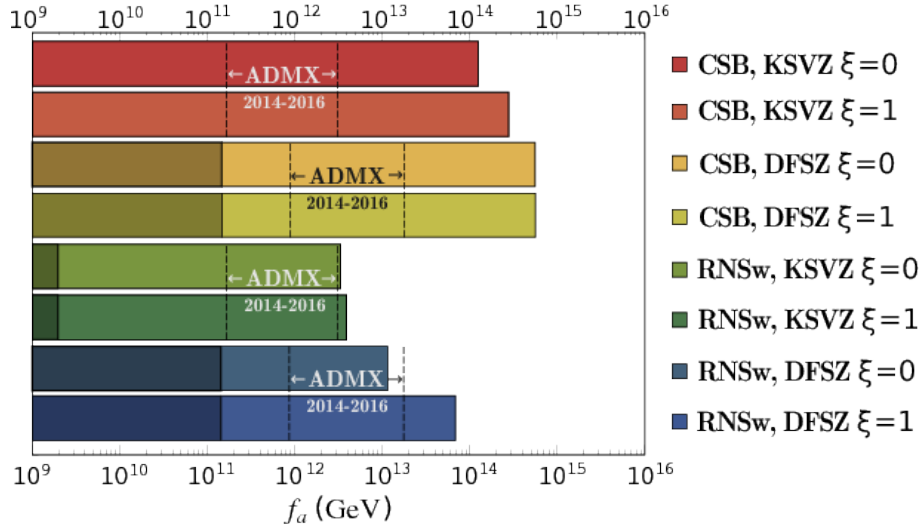


Figure 14: Range of f_a which is allowed in each PQMSSM scenario for the CSB and RNSw benchmark models. Darker-shaded regions indicate the range of f_a where $\theta_i > 3$ which might be considered unnatural. We also show the f_a range which is expected to be probed by the ADMX experiment in the next few years.

values ($\sim 10^9 - 10^{11}$ GeV) so that the DM abundance tends to be axion-dominated. This has important consequences for direct and indirect WIMP detection experiments since it anticipates a greatly reduced local abundance of WIMPs and hence diminished prospects for wino-like WIMP detection. This can actually allow for wino-like WIMP dark matter to evade the recent Fermi [61] searches for gamma ray emission from dwarf-spheroidal galaxies since in this case the expected event rate is expected to be reduced by a factor $(\Omega_{\tilde{W}} h^2 / 0.12)^2$.

A grand overview of our results is presented in Fig. 14, where we show the allowed range of f_a as a bar for each of the two benchmark points and for each of the eight SUSY PQ models considered. For all the models, no GUT scale values of f_a ($f_a \sim 10^{16}$ GeV) are allowed. This is due to the rather large value of $m_s \sim m_{3/2}$ in our benchmark models. In these cases, saxions always decay to SUSY particles and no entropy dilution of WIMPs and axions is possible (see Refs. [44, 34] for more details).

In addition to the SUSY KSVZ case with $SU(2)_L$ singlet heavy quark states which has been presented here, we have also investigated SUSY KSVZ models including $SU(2)_L$ doublet heavy quark states so that the axion superfield has couplings with $SU(2)_L$ gauge superfields. In the case of doublet heavy quarks, axino decays to the wino-like neutralino are not suppressed, even for $m_{\tilde{a}} < m_{\tilde{Z}_2}$. Therefore, there is no separate branch like the uppermost one in Fig. 2 and 3 and thus there are only two branches determined by $m_{\tilde{g}}$. The basic features of plots with doublet heavy quarks are similar to the case with singlet heavy quarks since the dominant axino decay mode is into gluinos for both cases. The allowed range of f_a values is extended only slightly for doublet KSVZ heavy quarks as compared to the case of singlet heavy quarks shown in this paper.

For sufficiently heavy axinos, all models shown in this paper are DM-allowed for the lower range of $f_a \sim 10^9 - 10^{12}$ GeV, since WIMPs are underproduced. In these cases, the remaining abundance is made up of axions. Even though one might expect a low axion abundance at low f_a in the case where the initial mis-alignment angle is $\theta_i \sim \mathcal{O}(1)$, due to anharmonicity effects the necessary axion abundance can always be obtained by taking $\theta_i \sim \pi$ [31]. In this case, one might wonder about fine-tuning of the axion abundance such that the axion fields sits atop the peak of its potential. Thus, for cases where $\theta_i > 3$, we shade these regions as darker in Fig. 14. The non-shaded regions may be more natural as far as the expected initial axion field value goes.

We should note that for KSVZ models, regions with $\theta_i < 3$ at low f_a occur only if the wino LSP constitutes more than $\sim 90\%$ of total CDM density since axion CO-production is very low for $f_a \lesssim 10^{10}$. Then, the CSB benchmark in the SUSY KSVZ model most naturally allows for the lowest f_a values while the CSB benchmark in the DFSZ model allows for the highest f_a values. The range of f_a values obtained for the RNSw benchmark is more constrained than the CSB case. The upper bounds on f_a for the two benchmark models are well-maintained even when the points are extended to model lines, as was shown for the DFSZ $\xi = 1$ case in Sec. 5.

Finally, we denote the range of f_a values which are expected to be probed in the next few years by the ADMX experiment [62]. The values shift between KSVZ and DFSZ models since the domain wall number $N_{\text{DW}} = 1$ for KSVZ and 6 for DFSZ and $m_a \simeq 0.62 \text{ eV}[10^7 \text{ GeV}/(f_a/N_{\text{DW}})]$. We also note that a possible ADMX technique of open resonators [63] may allow even lower values of f_a to be probed in the future.

Acknowledgments

We thank the William I. Fine Theoretical Physics Institute (FTPI) at the University of Minnesota for hospitality while the bulk of this work was completed. The computing for this project was performed at the OU Supercomputing Center for Education & Research (OSCER) at the University of Oklahoma (OU). A. L. thanks Fundação de Amparo à Pesquisa do Estado de São Paulo (FAPESP) for supporting this work.

References

- [1] L. Randall and R. Sundrum, Nucl. Phys. B **557**, 79 (1999); G. F. Giudice, M. A. Luty, H. Murayama and R. Rattazzi, JHEP **9812**, 027 (1998).
- [2] J. D. Wells, hep-ph/0306127.
- [3] N. Arkani-Hamed, A. Delgado and G. F. Giudice, Nucl. Phys. B **741**, 108 (2006) [hep-ph/0601041].
- [4] T. Moroi and L. Randall, Nucl. Phys. B **570**, 455 (2000).
- [5] G. Aad *et al.* [ATLAS Collaboration], Phys. Lett. B **716**, 1 (2012).
- [6] S. Chatrchyan *et al.* [CMS Collaboration], Phys. Lett. B **716**, 30 (2012).
- [7] H. Baer, V. Barger and A. Mustafayev, JHEP **1205**, 091 (2012).

- [8] H. Baer, V. Barger, D. Mickelson and M. Padeffke-Kirkland, *Phys. Rev. D* **89**, 115019 (2014).
- [9] J. D. Wells, *Phys. Rev. D* **71**, 015013 (2005).
- [10] N. Arkani-Hamed and S. Dimopoulos, *JHEP* **0506**, 073 (2005).
- [11] G. F. Giudice and A. Romanino, *Nucl. Phys. B* **699**, 65 (2004) [Erratum-ibid. *B* **706**, 65 (2005)].
- [12] N. Arkani-Hamed, S. Dimopoulos, G. F. Giudice and A. Romanino, *Nucl. Phys. B* **709**, 3 (2005).
- [13] B. S. Acharya, K. Bobkov, G. Kane, P. Kumar and D. Vaman, *Phys. Rev. Lett.* **97**, 191601 (2006); B. S. Acharya, K. Bobkov, G. L. Kane, P. Kumar and J. Shao, *Phys. Rev. D* **76**, 126010 (2007); B. S. Acharya, K. Bobkov, G. L. Kane, J. Shao and P. Kumar, *Phys. Rev. D* **78**, 065038 (2008); B. S. Acharya, G. Kane, E. Kuflik and R. Lu, *JHEP* **1105**, 033 (2011); for a review, see B. S. Acharya, G. Kane and P. Kumar, *Int. J. Mod. Phys. A* **27**, 1230012 (2012);
- [14] R. Kallosh and A. D. Linde, *JHEP* **0412**, 004 (2004).
- [15] M. Ibe and T. T. Yanagida, *Phys. Lett. B* **709**, 374 (2012); M. Ibe, S. Matsumoto and T. T. Yanagida, *Phys. Rev. D* **85**, 095011 (2012); B. Bhattacharjee, B. Feldstein, M. Ibe, S. Matsumoto and T. T. Yanagida, *Phys. Rev. D* **87**, 015028 (2013); J. L. Evans, M. Ibe, K. A. Olive and T. T. Yanagida, *Eur. Phys. J. C* **73**, 2468 (2013); J. L. Evans, M. Ibe, K. A. Olive and T. T. Yanagida, *Eur. Phys. J. C* **74**, 2931 (2014).
- [16] J. L. Evans, M. Ibe, K. A. Olive and T. T. Yanagida, arXiv:1412.3403 [hep-ph].
- [17] L. J. Hall and Y. Nomura, *JHEP* **1201**, 082 (2012).
- [18] L. J. Hall, Y. Nomura and S. Shirai, *JHEP* **1301**, 036 (2013).
- [19] G. B. Gelmini and P. Gondolo, *Phys. Rev. D* **74**, 023510 (2006).
- [20] B. S. Acharya, G. Kane, S. Watson and P. Kumar, *Phys. Rev. D* **80**, 083529 (2009).
- [21] R. Allahverdi, B. Dutta and K. Sinha, *Phys. Rev. D* **87** (2013) 075024.
- [22] H. Baer, K. Y. Choi, J. E. Kim and L. Roszkowski, *Phys. Rept.* **555**, 1 (2015).
- [23] G. L. Kane, P. Kumar, B. D. Nelson and B. Zheng, arXiv:1502.05406 [hep-ph].
- [24] H. Baer, R. Dermisek, S. Rajagopalan and H. Summy, *JCAP* **1007**, 014 (2010).
- [25] J. E. Kim, *Phys. Lett. B* **136**, 378 (1984).
- [26] R. D. Peccei and H. R. Quinn, *Phys. Rev. Lett.* **38**, 1440 (1977); S. Weinberg, *Phys. Rev. Lett.* **40**, 223 (1978); F. Wilczek, *Phys. Rev. Lett.* **40**, 279 (1978).
- [27] J. E. Kim, *Phys. Rev. Lett.* **43**, 103 (1979); M. A. Shifman, A. Vainshtein and V. I. Zakharov, *Nucl. Phys. B* **166**, 493(1980).
- [28] M. Dine, W. Fischler and M. Srednicki, *Phys. Lett.* **B104** (1981) 199; A. P. Zhitnitskii, *Sov. J. Phys.* **31** (1980) 260.
- [29] J. E. Kim and H. P. Nilles, *Phys. Lett. B* **138**, 150 (1984); E. J. Chun, J. E. Kim and H. P. Nilles, *Nucl. Phys. B* **370**, 105 (1992).
- [30] J. Preskill, M. Wise and F. Wilczek, *Phys. Lett. B* **120**, 127 (1983); L. F. Abbott and P. Sikivie, *Phys. Lett. B* **120**, 133 (1983); M. Dine and W. Fischler, *Phys. Lett. B* **120**, 137 (1983).

- [31] M. Turner, Phys. Rev. D **33**, 889 (1986); D. H. Lyth, Phys. Rev. D **45**, 3394 (1992); K. J. Bae, J. H. Huh and J. E. Kim, JCAP **0809**, 005 (2008); L. Visinelli and P. Gondolo, Phys. Rev. D **80**, 035024 (2009).
- [32] H. Baer, V. Barger, P. Huang, A. Mustafayev and X. Tata, Phys. Rev. Lett. **109**, 161802 (2012); H. Baer, V. Barger, P. Huang, D. Mickelson, A. Mustafayev and X. Tata, Phys. Rev. D **87**, no. 11, 115028 (2013).
- [33] H. Baer, V. Barger, P. Huang, D. Mickelson, M. Padeffke-Kirkland and X. Tata, arXiv:1501.06357 [hep-ph].
- [34] K. J. Bae, H. Baer, A. Lessa and H. Serce, JCAP **1410**, no. 10, 082 (2014).
- [35] M. Dine, A. Kagan and S. Samuel, Phys. Lett. B **243**, 250 (1990); A. Cohen, D. B. Kaplan and A. Nelson, Phys. Lett. B **388**, 588 (1996); N. Arkani-Hamed and H. Murayama, Phys. Rev. D **56**, 6733 (1997); T. Moroi and M. Nagai, Phys. Lett. B **723**, 107 (2013).
- [36] A. Pierce, Phys. Rev. D **70**, 075006 (2004).
- [37] A. Arvanitaki, C. Davis, P. W. Graham and J. G. Wacker, Phys. Rev. D **70**, 117703 (2004); A. Arvanitaki and P. W. Graham, Phys. Rev. D **72**, 055010 (2005).
- [38] B. S. Acharya, G. Kane and E. Kuflik, Int. J. Mod. Phys. A **29**, 1450073 (2014).
- [39] S. Kachru, R. Kallosh, A. D. Linde and S. P. Trivedi, Phys. Rev. D **68**, 046005 (2003).
- [40] K. Choi, A. Falkowski, H. P. Nilles, M. Olechowski and S. Pokorski, JHEP **0411**, 076 (2004); K. Choi, A. Falkowski, H. P. Nilles and M. Olechowski, Nucl. Phys. B **718**, 113 (2005); K. Choi, K. S. Jeong and K. i. Okumura, JHEP **0509**, 039 (2005).
- [41] A. Linde, Y. Mambrini and K. A. Olive, Phys. Rev. D **85**, 066005 (2012).
- [42] E. Dudas, A. Linde, Y. Mambrini, A. Mustafayev and K. A. Olive, Eur. Phys. J. C **73**, 2268 (2013).
- [43] K. J. Bae, H. Baer and A. Lessa, JCAP **1304**, 041 (2013).
- [44] K. J. Bae, H. Baer and E. J. Chun, JCAP **1312**, 028 (2013).
- [45] H. Baer and J. List, Phys. Rev. D **88**, 055004 (2013).
- [46] F. Paige, S. Protopopescu, H. Baer and X. Tata, [hep-ph/0312045](https://arxiv.org/abs/hep-ph/0312045); <http://www.nhn.ou.edu/~isajet/>
- [47] H. Baer, C. Balazs and A. Belyaev, JHEP **0203**, 042 (2002).
- [48] G. Belanger, F. Boudjema, A. Pukhov and A. Semenov, Comput. Phys. Commun. **185**, 960 (2014).
- [49] J. Pradler and F. Steffen, Phys. Lett. B **648**, 103 (1992).
- [50] K. Kohri, T. Moroi and A. Yotsuyanagi, Phys. Rev. D **73**, 123511 (2006).
- [51] K. -Y. Choi, J. E. Kim, H. M. Lee and O. Seto, Phys. Rev. D **77**, 123501 (2008); H. Baer, A. Lessa, S. Rajagopalan and W. Sreethawong, JCAP **1106**, 031 (2011).
- [52] H. Baer, S. Kraml, A. Lessa and S. Sekmen, JCAP **1011**, 040 (2010).
- [53] P. A. R. Ade *et al.* [Planck Collaboration], Astron. Astrophys. **571**, A16 (2014).
- [54] P. A. R. Ade *et al.* [Planck Collaboration], arXiv:1502.01589 [astro-ph.CO].

- [55] L. Covi, H. -B. Kim, J. E. Kim and L. Roszkowski, JHEP **0105**, 033 (2001); A. Brandenburg and F. D. Steffen, JCAP **0408**, 008 (2004); A. Strumia, JHEP **1006**, 036 (2010).
- [56] E. J. Chun, Phys. Rev. D **84**, 043509 (2011); K. J. Bae, K. Choi and S. H. Im, JHEP **1108**, 065 (2011); K. J. Bae, E. J. Chun and S. H. Im, JCAP **1203**, 013 (2012).
- [57] L. Hall, K. Jedamzik, J. March-Russell S. M. West, JHEP **1003**, 080 (2010)
- [58] T. Goto and M. Yamaguchi, Phys. Lett. B **276**, 103 (1992); E. J. Chun, J. E. Kim and H. P. Nilles, Phys. Lett. B **287**, 123 (1992);
- [59] E. J. Chun and A. Lukas Phys. Lett. B **357**, 43 (1995); J. E. Kim and M. -S. Seo, Nucl. Phys. B **864**, 296 (2012).
- [60] K. Jedamzik, Phys. Rev. D **74**, 103509 (2006).
- [61] M. Ackermann *et al.* (Fermi Collaboration), Phys. Rev. Lett. **107**, 241302 (2011); A. Geringer-Sameth and S. M. Koushiappas, Phys. Rev. Lett. **107**, 241303 (2011).
- [62] A. Kusenko and L. J. Rosenberg, arXiv:1310.8642 [hep-ph].
- [63] G. Rybka, A. Wagner, A. Brill, K. Ramos, R. Percival and K. Patel, Phys. Rev. D **91** (2015) 1, 011701.